Continuous Wave Simulations on the Propagation of Electromagnetic Fields Through the Human Head

Jeffrey M. Elloian*, Gregory M. Noetscher, Sergey N. Makarov, and Alvaro Pascual-Leone

***Abstract*—Characterizing the human head as a propagation medium is vital for the design of both on-body and implanted antennas and radio-frequency sensors. The following problem has been addressed: find the best radio-frequency path through the brain for a given receiver position—on the top of the sinus cavity. Two parameters, transmitter position and radiating frequency, should be optimized simultaneously such that 1) the propagation path through the brain is the longest; and 2) the received power is maximized. To solve this problem, we have performed a systematic and comprehensive study of the electromagnetic fields excited in the head by small on-body magnetic dipoles (small coil antennas). An anatomically accurate high-fidelity head mesh has been generated from the Visible Human Project data. The base radiator was constructed of two orthogonal magnetic dipoles in quadrature, which enables us to create a directive beam into the head. We have found at least one optimum solution. This solution implies that a distinct RF channel may be established in the brain at a certain frequency and transmitter location.**

***Index Terms*—Biomedical applications of electromagnetic radiation, electromagnetic propagation in absorbing media, medical diagnosis, mesh generation, surface waves.**

I. Introduction

OVER the past few years, there has been significant development in the field of wireless body area networks with numerous applications involving sensing or transmission of data from different points around or through the body [1], [2]. Clearly, there are multiple health-care advantages to being able to obtain information around the body remotely without dangerous and expensive, invasive procedures. A notable application is reviewed in [3], as the potential for the early diagnosis of Alzheimer's disease through the detection of internal changes of material properties is discussed. These problems require a signal path through the brain [1].

The human body is a unique transmission medium and may, in general, be described as a fairly dense, lossy, dielectric requiring special consideration. This paper investigates the fields excited by orthogonal coil antennas on the head, and optimizes the transmitter position and frequency (100 MHz to 1 GHz) to obtain a channel through the brain.

Manuscript received May 7, 2013; revised; accepted December 20, 2013. Date of publication January 9, 2014; date of current version May 15, 2014. *Asterisk indicates corresponding author.*

*J. M. Elloian is with the Department of Electrical and Computer Engineering, Worcester Polytechnic Institute, Worcester, MA 01605 USA (e-mail: jelloian@wpi.edu).

G. M. Noetscher and S. N. Makarov are with the Department of Electrical and Computer Engineering, Worcester Polytechnic Institute, Worcester, MA 01605 USA (e-mail: gregn@wpi.edu; makarov@wpi.edu).

A. Pascual-Leone is with the Berenson-Allen Center for Noninvasive Brain Stimulation, Beth Israel Deaconess Medical Center, Harvard Medical School, Boston, MA 02215 USA (e-mail: apleone@bidmc.harvard.edu).

Color versions of one or more of the figures in this paper are available online at http://ieeexplore.ieee.org.

Digital Object Identifier 10.1109/TBME.2013.2297871

II. Problem Statement

To remotely detect changes of internal organs, one can exploit the changes in magnitude, phase, and delay spread caused by shifts in the material properties. However, to observe such changes, one must first have a propagation path that transverses the organ of interest, the brain. Clearly, the effect of the material properties on this channel is proportional to the length of the path within the organ. However, in maximizing the path length, one must simultaneously maximize the received power. The greater the signal-to-noise ratio of the received signal, the more detail one can observe.

Given a fixed observation point, the optimal transmitter frequency and position is desired to produce a channel through the brain with the aforementioned properties. Several antenna types are considered and discussed before the selected orthogonal coil antenna is used to generate a directed beam on an anatomically accurate human head mesh. Simulations are then conducted to find this optimal channel.

III. Antenna Selection and Human Model

The human body is a lossy transmission medium, which presents several challenges in itself. Prior to the introduction of powerful simulation tools, researchers relied on theoretical derivations to guide experimentation. This is especially true for electromagnetic fields in biological tissue due to the difficulty involved in acquiring *in vivo* empirical results.

A. Antenna Selection

Selection of an antenna for the purpose of investigating propagation channels within the human body is not a trivial task. If one were to select a traditional dipole, the multipath caused by the boundaries between organs would cause the dispersed wave to be completely untraceable at the receiver, limiting the information that can be gathered about the channel. Furthermore, a dipole primarily radiates in the electric field, which is significantly affected by the permittivity of the human body. Although this can be mitigated by selecting a magnetic dipole or a loop, one would still need to find a way to "steer" the beam to a receiver on the head, providing information about a single, desired path.

There are several possible designs for wearable antennas, which typically are members of the patch family, as these can be

made conformal [4]. The objective of most wearable antennas is to transmit to a base station away from the body [4], [5]. Conversely, this project requires the antenna to able to transmit through the body.

The loop is a very simple option for selecting an antenna that can propagate through the body. A small loop or coil is very similar to a small dipole; however, it is horizontally polarized as opposed to vertically polarized [6]. This implies that a dipole would be radiating in E_θ, whereas a loop is radiating in H_θ. Fig. 2 illustrates the orientation of the H_θ with respect to two orthogonal coils (described in the following section). Therefore, the loop antenna should be less affected by dielectric loading. Unfortunately, the radiation pattern remains nearly the same as a dipole; thus, it can be difficult to properly distinguish the angle of arrival for internal channels [6].

An interesting variation of the classic loop is presented in [7]. The authors created segmented loop antennas to generate a uniform current distribution throughout the length of the antenna. Without segmentation (and the addition of the corresponding matching capacitance), there were regions with large specific absorption rate values. Once these so-called "hot-spots" appear, one must reduce the transmit power in order to avoid possible tissue damage [7]. This was of particular interest because the goal of the study was to improve the efficiency of the coupling that would power an implant.

Another variation is the fat arm spiral antenna, designed as means of wirelessly streaming images from an endoscopic capsule to a technician in real time, while providing more bandwidth (from 460 to 535 MHz) than traditional spiral or helix antennas. This additional bandwidth was provided by thickening the spiral. The antenna produces an omnidirectional radiation pattern vital to the particular case study, as the orientation of the capsule in the digestive tract relative to a fixed receiver is arbitrary [8].

A more complex approach is offered by Karathanasis and Karanasiou, who have developed a phased array-based reflector system to do beamforming within the human body. As opposed to a single radiating element, this system employs a 1.25 m $\times$ 1.2 m ellipsoidal cavity and changes the excitation phase to cause a local maximum in a given area, capable of inducing localized brain hyperthermia or treating hypothermia [9].

B. Orthogonal Coil Antennas

A possible solution to this problem was proposed in [3], where two orthogonal coil antennas were excited with a 90° phase difference to produce a single concentrated beam at 45°, without the need for a large or complicated array. This configuration, shown in Fig. 1, provides a maximum directivity of more than 10 dB, allowing one to use less transmitted power, while reducing interference caused by undesired reflections.

This special beamforming property only holds true when the loops are close to an air–dielectric interface that satisfies the quasi-static limit of $\sigma > \varepsilon\omega$ [10]. It is possible for a loop or dipole to generate a directive beam under the condition that the ratio of permititivies of the transmission media is large (greater than 4). With ε_r of air being 1 and ε_r of body tissues being on the order of 17–70, this is clearly applicable [11], [12]. Under

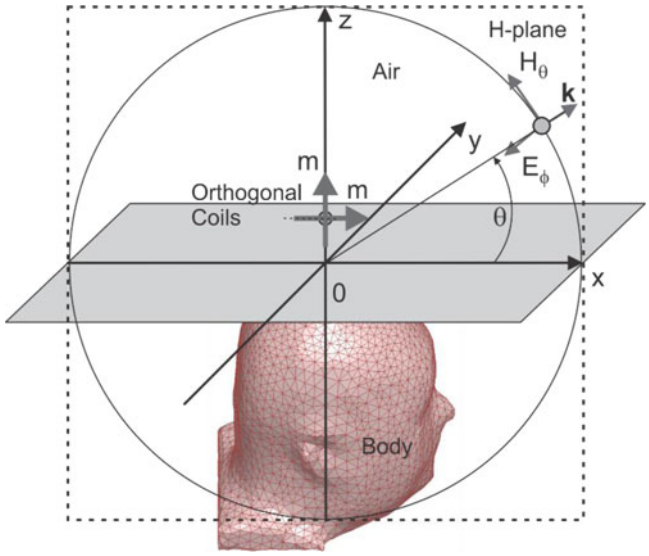

Fig. 1. Problem geometry for two orthogonal coils with respect to the **H** plane. The coils were modeled as loops with equivalent magnetic moments m.

this condition, and provided that the loops are excited close to the dielectric interface (i.e., the surface of the human body), the electric fields in the second medium (the body) in the H-plane (for horizontal and vertical loops, respectively) reduce to [10]:

$$E_{1x} = j\omega\mu_0 k_1 nm \left\{ \frac{|\sin(2\theta)|}{|\cos(\theta)| + j\,|\sin(\theta)|} \right\} \tag{1}$$

$$E_{2x} = \omega\mu_0 k_1 nm \left\{ \frac{\text{sign}(y)\,|\sin(2\theta)|}{|\cos(\theta)| + j\,|\sin(\theta)|} \right\} \tag{2}$$

where k_1 is the wavenumber through medium 1, $n = \sqrt{\varepsilon_2/\varepsilon_1}$ is the refractive index, y is the distance along the dielectric interface, and m is the magnetic dipole moment. These predict two main lobes for each dipole, centered at $\theta = 45°$, and $\phi = \pm 90°$ (the H-plane) [10]. By exciting the orthogonal coils 90° out of phase, it is possible to cause destructive interference in one lobe and constructive interference in the other, as shown in Fig. 2. The small size and highly directive pattern of this antenna make it an excellent candidate for this study.

C. Field Propagation

The most basic case of a time-varying harmonic field is the plane wave, which is an approximation of a propagating field far enough from the source that the wave front appears to be uniform. However, the intensity need not be uniform across the entire wave front. Indeed, the wavenumber can be a complex value, which is vital for the definition of the surface wave, as one can define a transverse wave impedance [13].

When waves come into contact with different media, the appropriate boundary conditions must be respected. This is a classic field closely tied with optics via Snell's law, giving rise to different modes. The most fundamental is the transverse electromagnetic mode, but waveguides operate on the principle of transverse electric, or transverse magnetic modes depending whether the **E** or the **H** field is perpendicular to the interface [14].

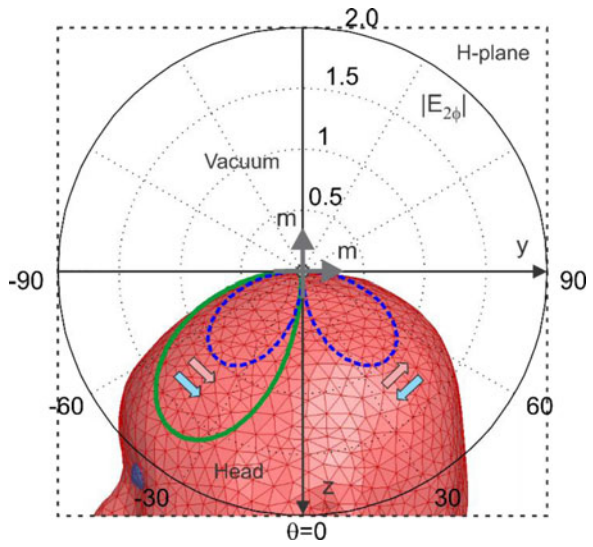

Fig. 2. Analytical electric field pattern with respect to the **H** plane for two orthogonal coils close to the human head. The coils are excited 90° out of phase (right) to null one beam and (left) to amplify the other.

Sommerfeld analytically characterized surface waves along a cylindrical wire, showing both the skin effect (with regards to the concentration of current within the wire) as well as the elliptical polarization of the electric field in the direction of propagation [15]. Less than a decade later, Zenneck introduced his controversial explanation of the surface waves observed in Sommerfeld's result [16]. Traditionally, it is accepted that radiation decays proportional to $\frac{1}{r}$ in the far field; however, Zenneck believed radios could transmit further by propagating through the ground via a so-called "Zenneck wave," which decays at a slower rate of $\frac{1}{\sqrt{r}}$. Although it was later determined that the ionosphere was acting as a reflector, permitting the transmission of electromagnetic waves over long distance, the existence of the Zenneck wave has long been debated [17].

The human body may be modeled as a planar set of layered, homogenous boundaries with the appropriate permittivities and conductivities [14]. By using a spatial transmission line propagation model, the transverse wave impedance of the ith boundary in the x-direction can be expressed by Lea *et al.* [13]:

$$Z_i = \frac{k_{x,i}}{\left(\frac{\omega\varepsilon_i - j\sigma_i}{\varepsilon_0}\right) k_0},\ (\text{TM});\ Z_i = \frac{\omega\mu_0}{k_{x,i}},(\text{TE}). \tag{3}$$

In general, the input impedance, from the perception of the boundary, must cancel to produce a surface wave on that boundary [13], [18]. The two major types of surface waves discussed are Norton and Zenneck waves. Norton waves are bound to a material interface and are described by the geometrical optics field subtracted from the radiating field [19]. Although an approximation intended for engineering purposes, the Norton wave equations describe the rate of decay. Assuming medium 2 is air, a Norton wave is given by [17]

$$E^s_{2z}(p,0) = \frac{j\omega\mu_0}{2\pi}\left(\frac{e^{jk_2p}}{p}\right) F_e \tag{4}$$

$$F_e = 1 + j\sqrt{\pi p}e^{-p}\left[1 - erf\left(j\sqrt{p}\right)\right]. \tag{5}$$

Note that p is the so-called "numeric distance," given by $p = jk_2\rho(\frac{k_2^2}{2k_1^2})$. Norton provides tables of F_e for various values of p in [20]. The rate of decay is proportional to e^{-p}, similar to the traditional far-field result, but the wave will be coupled to the surface as opposed to radiating into space.

On the other hand, the Zenneck wave can be expressed along the length of a boundary (again, medium 1 is the dielectric and medium 2 is air) as [17]:

$$E_{1z} = \frac{j\omega\mu_0 k_2}{k_1^2} A e^{jk_1 z} H_0^{(1)}(k_2\rho) \tag{6}$$

$$E_{2z} = \frac{j\omega\mu_0}{k_2} A e^{j\left(\frac{k_2^2}{k_1}\right)z} H_0^{(1)}(k_2\rho) \tag{7}$$

where $H_0^{(1)}$ are Hankel functions. Note that the Zenneck decays at a much slower rate of $\frac{1}{\sqrt{r}}$; however, the appropriate material parameters of the boundary must be selected for a Zenneck wave solution to exist. A more detailed discussion on these waves can be found in [17] and [19].

Based on the transverse impedances simulated by Lea *et al.* [13], it is unlikely that a Zenneck wave can be excited on the body with a short electric dipole. Considering that the body model used in [13] is inductive at lower frequencies, the conditions for the Norton or Zenneck surface waves could not be met, thus no TE surface waves could be observed below 5 GHz. Conversely, the fundamental TM mode produced surface waves, as the component of the electric field that is perpendicular to the surface is less affected by dielectric losses (severely attenuating any TE waves). Similarly, the presence of Norton waves was confirmed via simulation [13].

D. Human Body Meshes

In recent years, significant interest has been placed in the development of accurate human body meshes. Although it is easier to develop an analytical model for planar interfaces, such as the one shown in [13], the accuracy of such models is limited. The human body is far from a simple planar interface and the relatively high conductivity and permittivity of the lossy organs has a profound effect on the transmission characteristics [3]. Once one refines a model to include internal organs (more complex than planar homogeneous media), it is impractical to develop a full analytical model.

Fortunately, computational advances have resulted in detailed and reliable electromagnetic solution techniques such as finite difference time-domain, method of moments, and the finite element method (FEM). In order to use these powerful tools for medical analysis, one requires a mesh of the test subject. A mesh is a series points that make up triangles and tetrahedra to form a 3-D structure that closely approximates the object in question. As one would expect, the finer the resolution of the mesh, the larger the mesh, and the longer the computation time. With accurate, computationally feasible meshes of the human body, it would be possible to run a variety of EM simulations to advance science and medicine, minimizing the number of dangerous tests that need to be done to live subjects. Examples

of commercially available human body models can be found in [21]–[25].

Custom meshes were constructed for this project from the raw cryoslice data provided by the Visible Human Body Project [26]. The images were produced by photographing slices of the axial plane of a female subject at a resolution of 2048×1216 pixels, with each pixel having an area of $0.33\ \mathrm{mm}^2$.

Organs, including the brain, skull, jaw, tongue, and spine, were identified in pertinent cryoslices and hand-segmented using ITK-Snap [28], meshed, and imported into MATLAB. This time-consuming process described in [3] results in large, fine resolution triangular surface meshes. Each of these was further simplified using surface-preserving Laplacian smoothing [29] to enable fast, yet accurate simulations. Resulting models have 1000–12 000 triangles per structure and mesh description via the NASTRAN file format [30], [31] allows users to import into custom and commercial simulation software packages. In this way, all meshes were imported into Ansys' High Frequency Structural Simulator (HFSS) v. 14, a commercially available FEM electromagnetic simulation suite, and the mesh checking tools resident in this package were utilized to check each model for manifoldness, intersection, and other relevant properties.

Creation of the cerebrospinal fluid (CSF), a highly conductive liquid that entirely encompasses the brain and is vital to the accuracy of any electromagnetic simulation involving the head, followed a slightly different process. Since the brain can move about in the CSF, certain cryoslices depicted the brain directly adjacent to the skull with no space allocated for the CSF. Therefore, the brain mesh model was converted via 3-D Delaunay tessellation to a strictly convex shape. Such an operation will allow for all nonconvex cavities on the brain surface to be filled with the CSF. This boundary triangular mesh may be extracted from the tetrahedral mesh and scaled to match an expected 2.5-mm-thick CSF layer.

The final mesh used in these simulations is a refined version of the one presented in [3] with additional organs and tissues shown in Fig. 3 to provide a more accurate model of the human head. Although not directly intersecting the *YZ* plane in Fig. 3, the eyes are also included in the simulations. The brain is considered a single combined mass, whose permittivity as also given in [27]. The ventricles in the brain are assumed to be filled with CSF.

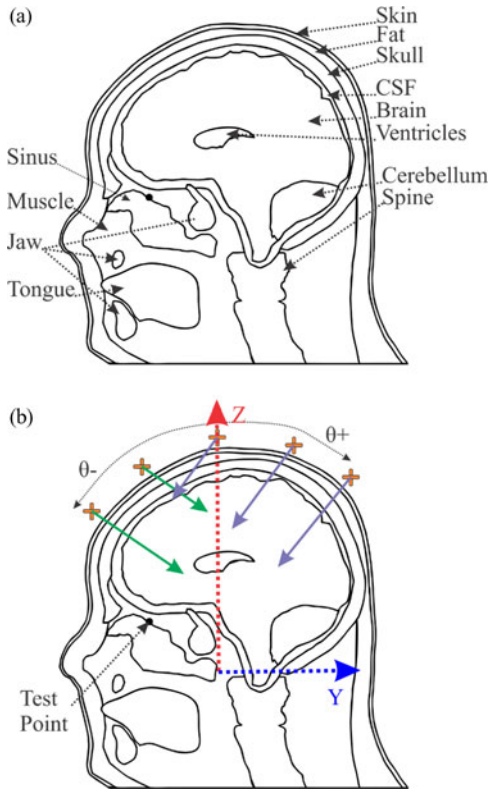

Fig. 3. Cross section of the sagittal (*YZ*) plane of the human head model. (a) Locations of included organs. (b) Examples of antenna locations with respect to θ. The phase of the excitation was adjusted such that the 45° beam transverses the head, as indicated by the green and purple arrows.

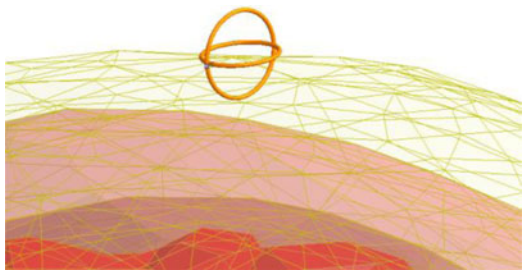

Fig. 4. Close-up view of the two orthogonal loop antennas used in the following simulations. Only the skin, skull, CSF, and brain meshes are shown for clarity.

IV. Modeling Results

Simulations were performed using HFSS. The meshes used to generate the model were constructed from data provided by the U.S. National Library of Medicine [26]. After segmenting and meshing individual organs of the female human head model, the results were imported into HFSS and assigned their respective dielectric constant (ε_r) and conductivity (σ), which were obtained from [27]. The frequency dependence of both of these material properties was accounted for in the simulations.

As an extension of the work done in [3] which utilized pulses, the finite element solver in HFSS was used to conduct continuous wave (CW) simulations at specific frequencies. The coils were constructed of 0.4-mm-thick wire, and were 7 mm in diameter. In order to assist in characterizing the human head channel as a transmission medium, the transmitting antenna was positioned around the head in a spherical-based coordinate system as shown in Fig. 1. The distance from the center of mass of the head to the center of the coil antennas was adjusted such the edges were approximately 1 mm from the surface. This adjustment was necessary because the human head is clearly not a perfect sphere, and the coils were to remain close to but not intersecting the dielectric interface. An example is shown in Fig. 4.

At each labeled point in Fig. 3, the antenna was laterally translated (without rotation) and excited in a manner that would direct the beam through the head. The testing points extended from $-60°$ to $+60°$ in steps of 5° in either cut-plane (sagittal *YZ* and coronal *XZ* planes) for a total of 49 different testing points. Only the results for the sagittal plane are considered in

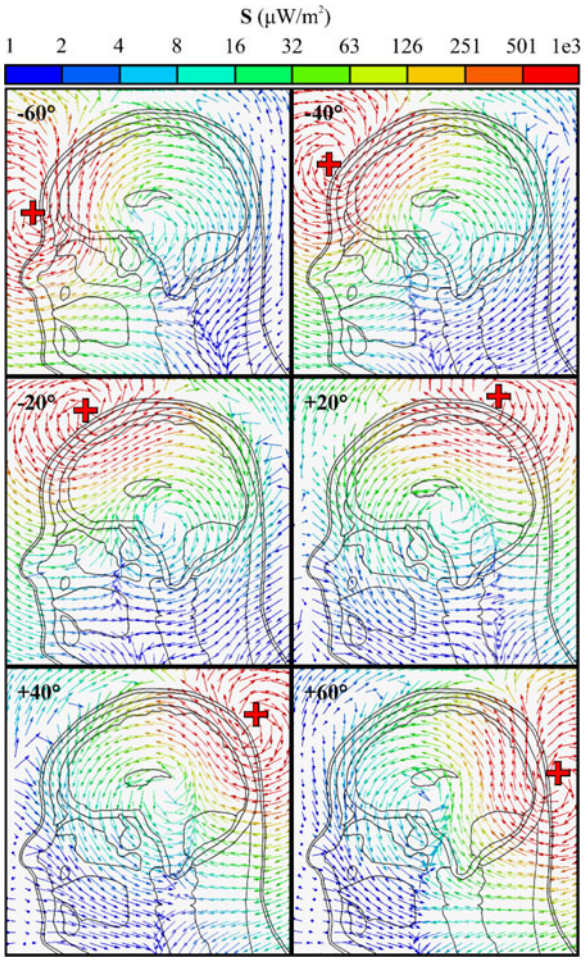

Fig. 5. Magnitude and direction of the Poynting vector for selected antenna positions at 100 MHz. The red crosses show the locations of the transmitter (the size is exagerated for clarity).

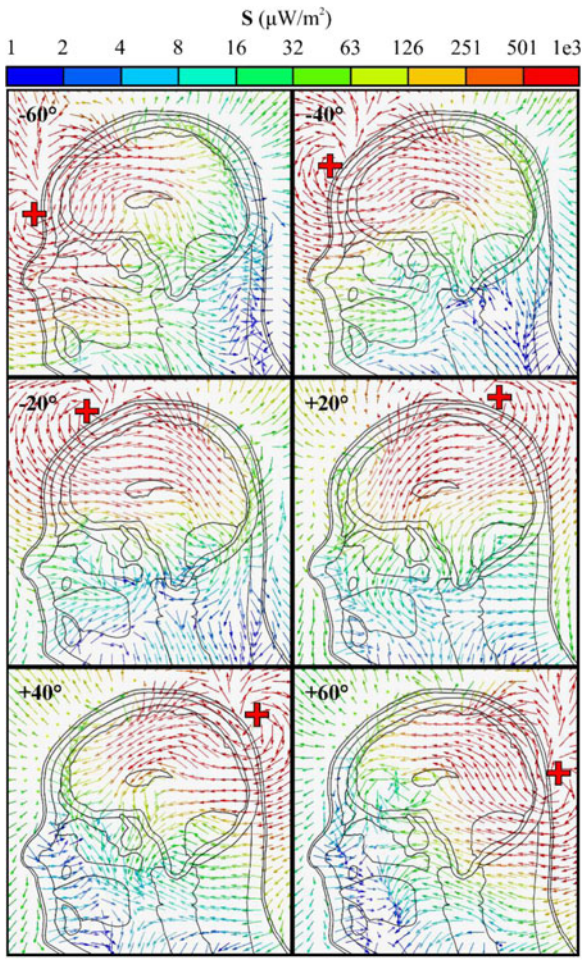

Fig. 6. Magnitude and direction of the Poynting vector for selected antenna positions at 500 MHz.

this paper, as the coronal plane is more symmetric and did not provide a feasible point to extract the fields.

For brevity, the complete set of calculations is not included in this paper. Instead, only the most interesting and useful field plots are displayed. It is important to note that the organs within the human head have a high relative dielectric constant (>50), which results in a slower phase velocity. This delay is intentionally used in [3] to remotely detect changes within the body; however, it also scales the magnitude of the received electric field. In order to more easily detect the propagation paths within the head, the Poynting vector ($\boldsymbol{S} = \boldsymbol{E} \times \boldsymbol{H}^*$) is plotted on a logarithmic scale. This shows the direction of power flow and eliminates the oscillating standing waves.

A. *Poynting Vector at Selected Frequencies*

Again, the goal of this study is to establish a channel though the human head. Not only must the power penetrate the head and travel through the brain, it must be extracted. To achieve this objective, two design variables must be optimized: the location measured from the center of the head (given as the angle θ) and the frequency of excitation f. Fig. 5 shows the propagation of power at 100 MHz. At low frequencies the wavelength in free space is over a meter, and even in the brain (with one of the highest dielectric constants of $\varepsilon_r = 88.9$ at 100 MHz), the wavelength is still greater than 300 mm [27]. The resulting Poynting vector plots resemble those of the near field of the orthogonal coils in free space.

Mid-range frequencies, such as 500 MHz, cause the wavelength to be closer to the Fresnel region and allow the antenna to demonstrate the targeted directive pattern described in [10], as shown in Fig. 6. The CSF, with $\varepsilon_r = 70.1$ and $\sigma = 2.28\frac{S}{m}$ at 500 MHz, begins to act like the walls of a waveguide around the brain [27]. Depending on the direction of excitation, this effect steers the beam along the inner contour of the brain to either the cerebellum or the sinus cavity. Unfortunately, at higher frequencies the difference in ε causes a much larger angle of refraction at the sinus(air)/muscle interface, making the field more difficult to recover.

As one increases the frequency, the problems observed in Fig. 6 begin to escalate. Fig. 7 illustrates the Poynting vector for the orthogonal coils being excited at 1 GHz. The 45° beam is still clearly present, albeit curved by the aforementioned waveguide effect of the CSF, but reflections from this boundary begin to eliminate the propagating component of the wave. This

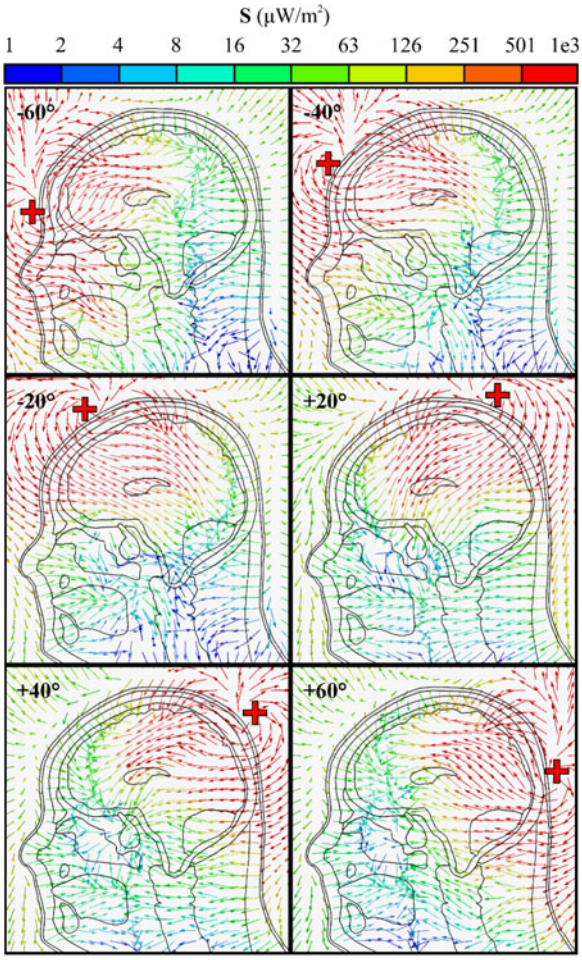

Fig. 7. Magnitude and direction of the Poynting vector for selected antenna positions at 1 GHz.

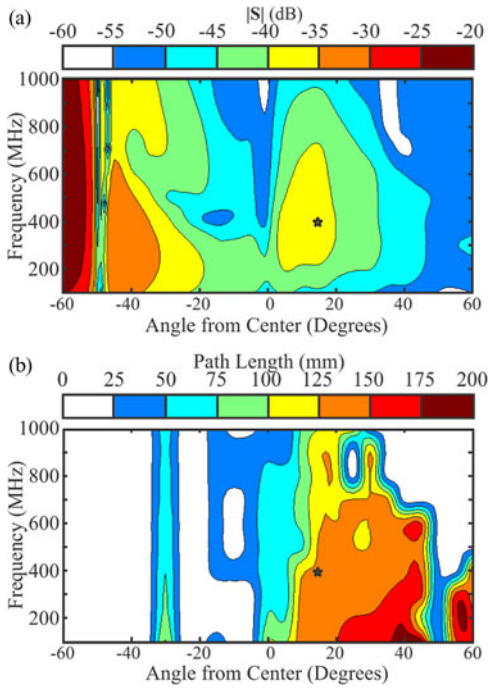

Fig. 8. (a) Magnitude of the Poynting vector evaluated at the test point above the sinus cavity as shown in Fig. 3 for different excitation positions and frequencies. (b) Length of the path of power propagation through the brain. The star indicates the selected optimal compromise in maximizing the received power and propagation distance through the brain (at $\theta = +15^\circ$ and $f = 400$ MHz).

cancellation would make signal extraction very challenging, as there is little to no forward propagating power through the brain that exits the head.

B. Optimized Transmitter Location

The ideal transmission channel would propagate through a long path within the brain and be received with the maximum power transfer through this path. A longer propagation path through the brain will experience a greater effect in attenuation and phase velocity due to abnormalities in the material properties in the brain. Furthermore, increasing this length would help negate the effects the short distances required to enter or leave the brain. Clearly, maximizing the power received (i.e., concentrating the beam) allows one to more easily observe these changes in the presence of noise.

This now becomes an optimization problem, where one must maximize the path length through the brain without compromising received power. A test point was selected on top of the sinus cavity [as shown in Fig. 3(b)] to measure the received fields. Although similar study could be preformed with a more practical receiver on the tongue, the sinus cavity destroys all paths to the tongue at higher frequencies.

The transmitting coils were moved from $\theta = -60^\circ$ to $+60^\circ$ in steps of 5° at a constant distance of approximately 1 mm to the surface of the head, as depicted in Fig. 3(b). At each transmission point, the fields were simulated for excitations from 100 MHz to 1 GHz in steps on 100 MHz. The magnitude of the Poynting vector at the test point shown in Fig. 3(b) is summarized in Fig. 8(a).

The disproportionately large magnitudes near -60° in Fig. 8(a) are caused by the close proximity of the transmitter on the front of the head and the test point in the sinuses. These values are less relevant as there is virtually no path through the brain. Near $+15^\circ$, the magnitude reaches a local plateau between -40 and -35 dB before sharply dropping. Fig. 9 is an example of antenna located at this location. One may note that the high intensity is caused by the waveguide properties of the CSF channeling the power into the sinus cavity at frequencies between 200 and 600 MHz. Higher frequencies at this position begin to suffer from reflection, reducing the magnitude of received Poynting vector.

Fig. 8(b) plots the path length through the brain on the same axes as Fig. 8(a). We define the propagation path to exclusively be the curved distance (following the vectors), not the perpendicular distance, from the transmitter to the test point. Each distance was graphically calculated using vector plots such as those in Figs. 5–9. Only the portion of this curve that is inside the brain is considered, and cases that did not have a path from the antenna to the test point via the brain were discarded as having a path length of 0.

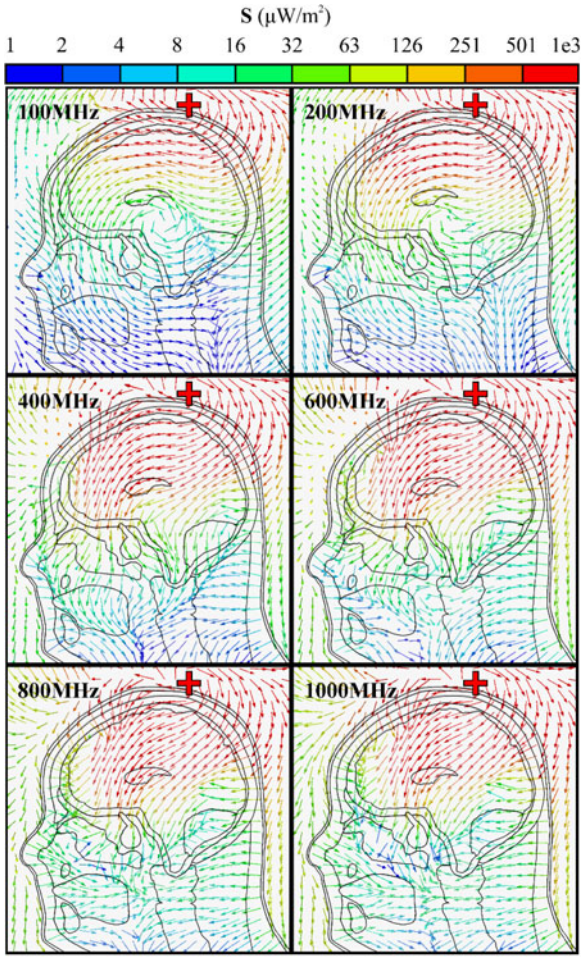

Fig. 9. Magnitude and direction of the Poynting vector for an antenna placed at $\theta = +15^\circ$ at selected frequencies.

The optimal location and frequency for the transmitter is problem dependent, as one must find a compromise between a long propagation path through the brain and high received power. We selected the starred point in Fig. 8 (at $\theta = +15^\circ$ and $f = 400$ MHz), where $|\boldsymbol{S}| > -40$ dB, and the path length through the brain is at least 125 mm. Other transmitter locations and frequencies produced a shorter path, or the received power was too low to be feasibly measured with noise.

V. Discussion and Conclusion

The simulations presented in this paper demonstrate the existence of a channel through the brain to the sinus cavity. By exciting orthogonal coil antennas in quadrature, a directed beam can be generated and steered through a dielectric medium. By adjusting the transmitter position and excitation frequency, an optimal path through the brain was found.

The model simulated in [3] demonstrated faint, yet distinct surface waves along the head. No surface waves were observed on the new mesh. In order to better classify the fields on this earlier model, the magnitude of the electric field was simulated following a segmented line along the surface of the head. The observed waves could be described by the Norton wave with a rate of decay proportional to e^{-r}, which is much slower than the expected rate of $\frac{1}{r}$ [17].

When the brain undergoes any form of serious trauma, through either injury or the development of a tumor, the physical and electric properties change accordingly. Recent studies indicate that different levels of blood content, potentially caused by burst blood vessels in the head, will lead to different dielectric properties [32], [33]. The channel established earlier in this text can be used to detect such abnormalities.

A CW is ideal for detecting volumetric changes of the brain. It is narrowband, straightforward to produce and measure, and provides a clear phase reference. Conversely, a broadband pulse would provide additional frequency diversity, allowing one to determine the existence of small objects, such as localized lacuna tumors in the brain. This is possible because the additional frequencies allow one to resolve more paths, thus obtaining additional information from the multipath characteristics of the channel. Broadband pulse simulation is beyond the scope of this study. An excellent example of such an analysis is provided in [32], but requires complex signal processing and 72 antennas to image the entire head. On the contrary, the CW technique shown here allows for simple and rapid detection of any general abnormality in the brain by observing the integral characteristics of the wave. This, perhaps, could be used as a screening measure to determine if more in-depth analysis is needed.

The meshes used in this study were improved from those in [3] from both an anatomical and material perspective. Previous versions did not include separate layers for the fat, muscle, and other organs. Furthermore, in this new study, all material properties were obtained from [27], the internationally recognized Foundation for Research on Information Technologies in Society. However, the previous model still illustrates a similar path through the brain to the tongue at a similar transmission position. This implies that the existence of the path may be robust to material changes. One may need to tune the exact frequency and position, but there should be at least one acceptable transmission path. The variance in the conditions for generating these paths for different head models would be a worthwhile avenue of research for conducting practical microwave tomography.

Acknowledgment

This paper would not have been possible without meshing assistance provided by A. T. Htet of Worcester Polytechnic Institute. The authors would also like to thank Dr. S. Louie of Ansys for her advice regarding the simulation software and methods. Dr. Rao of the MITRE Corporation also provided invaluable advice. All simulations were performed at the Worcester Polytechnic Institute.

References

[1] P. S. Hall, Y. Hao, and S. L. Cotton, "Progress in antennas and propagation for body area networks," in *Proc. Int. Symp. Signals Syst. Electron.*, Sep. 17–20, 2010, vol. 1, pp. 1–7.

[2] A. Gupta and T. D. Abhayapala, "Body area networks: Radio channel modelling and propagation characteristics," in *Proc. Australian Commun. Theory Workshop*, Jan. 30–Feb. 1, 2008, pp. 58–63.

[3] G. Noetscher, A. Htet, J. Elloian, S. Makarov, F. Sciré-Scappuzzo, and A. Pascual-Leone, "Detecting *in vivo* changes of electrical properties of cerebral spinal fluid using microwave signals from small coil antennas—Numerical simulation," in *Proc. IEEE Signal Process. Med. Biol. Symp.*, Dec. 2012, pp. 1–6.

[4] N. H. M. Rais, P. J. Soh, F. Malek, S. Ahmad, N. B. M. Hashim, and P. S. Hall, "A review of wearable antenna," in *Proc. Loughborough Antennas Propag. Conf.*, Nov. 16/17, 2009, pp. 225–228.

[5] J. C. G. Matthew, B. Pirollo, A. Tyler, and G. Pettitt, "Body wearable antennas for UHF/VHF," in *Proc. Loughborough Antennas Propag. Conf.*, Mar. 17/18, 2008, pp. 357–360.

[6] C. Balanis, *Antenna Theory*, 3rd ed. Hoboken, NJ, USA: Wiley-Interscience, 2005, pp. 231–265.

[7] M. Mark, T. Bjorninen, L. Ukkonen, L. Sydanheimo, and J. Rabaey, "SAR reduction and link optimization for mm-size remotely powered wireless implants using segmented loop antennas," in *Proc. IEEE Top. Conf. Biomed. Wireless Technol., Netw., Sens. Syst.*, Jan. 16–19, 2011, pp. 7–10.

[8] S. Lee and Y. Yoon, "Fat arm spiral antenna for wideband capsule endoscope systems," in *Proc. IEEE Radio Wireless Symp.*, Jan. 10–14, 2010, pp. 579–582.

[9] K. Karathanasis and I. Karanasiou, "Combining reflector focused and phased array beamforming for microwave diagnosis and therapy," in *Proc. IEEE 12th Int. Conf. Bioinformat. Bioeng.*, Nov. 11–13, 2012, pp. 223–226.

[10] S. Makarov and G. Noetscher, "Directional in-quadrature orthogonal-coil antenna and an array thereof for localization within a human body in a Fresnel region," in *Proc. IEEE Int. Symp. Antennas Propag. Soc.*, Jul. 8–14, 2012, p. 1/2.

[11] J. Kim and Y. Rahmat-Samii, "Implanted antennas inside a human body: Simulations, designs, and characterizations," *IEEE Trans. Microw. Theory Tech.*, vol. 52, no. 8, pp. 1934–1943, Aug. 2004.

[12] C. Gabriel S. Gabriel, "Compilation of the dielectric properties of body tissues at RF and microwave frequencies," *Armstrong Lab.* (1996). [Online]. Available: http://www.brooks.af.mil/AFRL/HED/hedr/reports/dielectric/home.html

[13] A. Lea, P. Hui, J. Ollikainen, and R. Vaughan, "Propagation between on-body antennas," *IEEE Trans. Antennas Propag.*, vol. 57, no. 11, pp. 3619–3627, Nov. 2009.

[14] F. Ulaby, E. Michielssen, and U. Ravaioli, *Fundamentals of Applied Electromagnetics*, 6th ed. Upper Saddle River, NJ, USA: Pearson Education, 2010.

[15] A. Sommerfeld, "Electromagnetic waves near wires," *Wied. Ann.*, vol. 67, pp. 223–290, 1899.

[16] J. Zenneck, "Ueber die fortplanzung ebener electromagnetischen wellen laengs einer ebenen leiterflaeche und ihre bezeihung zur drahtlosen telegraphie," *Ann. Phys.*, vol. 23, pp. 846–866, 1907.

[17] R. King and M. Brown, "Lateral electromagnetic waves along plane boundaries: A summarizing approach," *Proc. IEEE*, vol. 72, no. 5, pp. 595–611, May 1984.

[18] A. Lea, P. Hui, J. Ollikainen, and R. Vaughan, "Theory of propagation for direct on-body wireless sensor communications," in *Proc. 2nd IET Seminar Antennas Propag. Body-Centric Wireless Commun.*, Apr. 2009, pp. 1–5.

[19] J. Wait, "The ancient and modern history of EM ground-wave propagation," *IEEE Antennas Propag. Mag.*, vol. 40, no. 5, pp. 7–24, Oct. 1998.

[20] K. A. Norton, "The propagation of radio waves over a plane earth," *Nature*, vol. 135, pp. 954–955, 1935.

[21] *Ansoft Human Body Model, Ansoft Human Body Model Documentation,* Ansys, Canonsburg, PA, USA, 2012.

[22] Computer Simulation Technology. (Mar. 2013). HUGO Human Body Model. . [Online]. Available: http://www.cst.com/Content/Applications/Article/HUGO+Human+Body+Model

[23] Speag. (2012). "High Resolution Phantom Models," [Online]. Available: http://www.speag.com/products/semcad/applications/medical-technology-simulations/high-resolution-phantom-models

[24] C. Penney, (Jan. 23, 2008). "Computation of fields and SAR for MRI with finite-difference, time-domain software," [Online]. Available: http://www.remcom.com/storage/downloads/publications/computation%20of%20fields%20and%20sar%20for%20mri_mw%20journal%20dec%2007_final.pdf

[25] FEKO. (2013). "Bio-Electromagnetics," [Online]. Available: http://www.feko.info/applications/Bio-Electromagnetics

[26] U.S. National Library of Medicine. The Visible Human Project®. (2000). [Online]. Available: http://www.nlm.nih.gov/research/visible/visible_human.html

[27] [IT'IS Foundation. (2012). "Tissue Properties," IT'IS Foundation. [Online]. Available: http://www.itis.ethz.ch/itis-for-health/tissue-properties/database/dielectric-properties

[28] P. A. Yushkevich, J. Piven, H. C. Hazlett, R. G. Smith, S. Ho, J. C. Gee, and G. Gerig, "User-guided 3D active contour segmentation of anatomical structures: Significantly improved efficiency and reliability," *Neuroimage*, vol. 31, no. 3, pp. 1116–1128, Jul. 1, 2006.

[29] J. Vollmer, R. Mencl, and H. Müller, "Improved Laplacian smoothing of noisy surface meshes," *Comput. Graph. Forum*, vol. 18, no. 3, pp. 131–138, Sep. 1999.

[30] MD NASTRAN INPUT, Copyright© 2010 MSC.Software Corporation. (2010). [Online]. Available: http://www.aero.polimi.it/∼lanz/bacheca/downloads/cost/aa10_11/MD_Nastran_Input.pdf

[31] La syntaxe particulière de NASTRAN. (2013), [Online]. Available: https://moodle.polymtl.ca/pluginfile.php/120548/mod_page/content/3/Travaux_pratiques/TP1/suppl_labo_sem0.pdf

[32] D. Ireland and M. Bialkowski, "Microwave head imaging for stroke detection," *Progress Electromagn. Res. M*, vol. 21, pp. 163–175, 2011.

[33] U. Serguei, Y. Semenov, and D. R. Corefield, "Microwave tomography for brain imaging: Feasibility assessment for stroke detection," *Int. J. Antennas Propag.*, vol. 2008, 2008, pp. 1–8.

Authors' photographs and biographies not available at the time of publication.